Full Text View

The Inner Shelf Response to Wind-Driven Upwelling and Downwelling–[*]

Jay A. Austin

Center for Coastal Physical Oceanography, Old Dominion University, Norfolk, Virginia

Steven J. Lentz

Woods Hole Oceanographic Institution, Woods Hole, Massachusetts

ABSTRACT

A two-dimensional numerical model is used to study the response to upwelling- and downwelling-favorable winds on a shelf with a strong pycnocline. During upwelling or downwelling, the pycnocline intersects the surface or bottom, forming a front that moves offshore. The characteristics of the front and of the inner shelf inshore of the front are quite different for upwelling and downwelling. For a constant wind stress the upwelling front moves offshore at roughly a constant rate, while the offshore displacement of the downwelling front scales as $(t)^{1/2}$ because the thickness of the bottom layer increases as the front moves offshore. The geostrophic alongshelf transport in the front is larger during downwelling than upwelling for the same wind stress magnitude because the geostrophic shear is near the bottom in downwelling as opposed to near the surface in upwelling. During upwelling, weak stratification is maintained over the inner shelf by the onshore flux of denser near-bottom water. This weak stratification suppresses vertical mixing, causing a small reduction in stress at mid depth that drives a weak cross-shelf circulation over the inner shelf. For constant stratification, the inner shelf stratification and cross-shelf circulation are stronger. During downwelling on an initially stratified shelf, the inner shelf becomes unstratified because the very weak cross-shelf circulation forces lighter water under denser, driving convection which enhances the vertical mixing. As a result the stress is nearly constant throughout the water column and the cross-shelf circulation is slightly weaker than in the initially unstratified case. The downwelling response is essentially the same for the constant stratification and the two-layer cases. Model runs including the evolution of a passive tracer indicate that the inner shelf region acts as a barrier to cross-shelf transport of tracers from the coastal boundary to farther offshore and vice versa, due to strong vertical mixing and weak cross-shelf circulation in this region.

Options:
- Create Reference
- Email this Article
- Add to MyArchive
- Search AMS Glossary

Search CrossRef for:
- Articles Citing This Article

Search Google Scholar for:
- Jay A. Austin
- Steven J. Lentz

1. Introduction

Wind-driven currents play a major role in circulation in coastal regions around the world (Smith 1995). Upwelling and downwelling circulations are of particular interest because of the role their secondary, cross-shelf, circulation plays in redistributing not only heat and salt (and hence density) but also nutrients and biological fields. In this paper, we consider the response to upwelling- and downwelling-favorable winds of a shelf that initially has a strong midwater pycnocline. This is a typical condition on many shelves during summer. We use a numerical model to investigate the response from a process-oriented perspective. Idealized bathymetry, initial stratification, and forcing are used, as opposed to more realistic conditions, in order that simple analytic scalings can be derived and applied to a wide range of conditions. Our specific focus will be on the "inner shelf," defined here as the region inshore of the front formed when upwelling or downwelling winds move the pycnocline offshore.

The formation and offshore displacement of the upwelling or downwelling front partitions the shelf into dynamically distinct regions with different stratification. In both upwelling and downwelling, full Ekman transport develops in the region offshore of the upwelling or downwelling front because the strong stratification (and hence, weak vertical mixing) of the pycnocline acts to "insulate" the surface and bottom layers from each other. Onshore of the front, the stratification is relatively weak and the surface and bottom Ekman layers typically interact, causing a significant reduction in the net cross-shelf transport. The necessity for this divergence was recognized by Ekman (1905), though in that case the reduction is simply attributed to a reduction in depth, as his model assumed a constant eddy viscosity. Lentz (1995) used this divergence as the definition of the inner shelf, calling it "the region characterized by cross-shelf divergence in the (surface) Ekman transport due to the interaction of the surface and bottom boundary layers." As the water needs to be deep before the surface and bottom boundary layers are separate in weakly stratified or unstratified waters, the region inshore of the upwelling or downwelling front is, for all practical purposes, equivalent to the inner shelf under this definition. Defining the inner shelf as the region inshore of the upwelling or downwelling front is a more practical definition to apply to field observations, as these fronts are considerably easier to observe than divergence in the surface Ekman transport (Lentz 2001). The fact that the eddy viscosity depends on flow and stratification, and hence is not constant, makes it difficult if not impossible to classify regions of the shelf in terms of the Ekman number.

The development of progressively more complex turbulence closure models has allowed numerical models to more faithfully reproduce the role of mixing in upwelling systems. Models such as those of Hamilton and Rattray (1978), Foo (1981), and Kundu (1984) all considered two-dimensional upwelling of a stratified fluid over a flat bottom or a deep but weakly sloping bottom. With a configuration similar to the one used in this study, Allen et al. (1995) and Allen and Newberger (1996) used the Princeton Ocean Model to study the response to upwelling-favorable and downwelling-favorable wind stress, respectively. The parameters used in their study were motivated by bathymetric and hydrographic conditions typical of the west coast of North America, relatively constant stratification over a narrower, steeper shelf. In this study, the focus is on conditions more typical of the North American East Coast; specifically, a wide, shallow shelf and stratification characterized by a strong vertically localized pycnocline (Austin and Lentz 1999). In addition, the focus of the Allen et al. (1995) and Allen and Newberger (1996) paper was on the entire shelf response, whereas we will focus more on the inner shelf response.

This study, as with most other two-dimensional models, leaves out several potentially important sources of variation in order to focus on the wind-driven response alone, and in particular the response of the inner shelf. Any study of a realistic upwelling event must include alongshore variation, as inevitably exists in nature. Alongshore gradients in effective alongshore wind stress, bathymetry, or stratification can lead to differences in alongshore transport, which serve to build alongshore pressure gradients counter to the wind stress. These pressure gradients eventually drive cross-shelf circulation that can bring the pycnocline back onshore. The study also does not consider the role of the specific mixing parameterization chosen. However, the most important aspect of the mixing appears to be the strong inverse dependence of eddy viscosity on stratification, which is a feature common to most of the more sophisticated mixing parameterizations. Finally, this study does not consider the role of surface heating, to which relaxation after upwelling has been partially attributed (Send et al. 1987). However, this does not account for the fact that the salinity field is also observed to relax, suggesting that the alongshore pressure gradient is likely the most important omission in this work.

The paper proceeds as follows. In section 2, the numerical model is briefly outlined and the configuration described. Section 3 contains a description of "base case" upwelling and downwelling responses, as well as consideration of the dependence of the response on the model parameters. Section 4 is a discussion of some related topics, specifically the response of a continuously stratified shelf and the behavior of passive tracers on the inner shelf. A short summary of results follows in section 5.

2. The numerical model

In this section the numerical model and the physical parameters used in the model are described, including the "base case" model run, which is the focus of section 3.

a. Description of the model

The numerical model used is the Princeton Ocean Model (POM: Blumberg and Mellor 1987). POM is a hydrostatic, free-surface, numerical model, written for the study of coastal circulation, and has been used by many investigators in the past. The model is run in a two-dimensional channel configuration eliminating alongshelf variability. Vertical turbulent mixing is parameterized with the Mellor–Yamada level 2.5 turbulence submodel (Mellor and Yamada 1982), with the modification limiting the mixing length scale described by Galperin et al. (1988). In addition, there is a background vertical eddy viscosity and diffusivity of $v = 2 \times 10^{-5}$ m^2 s^{-1} and a constant horizontal eddy viscosity and diffusivity of $A_M = A_H = 2$ m^2 s^{-1}.

1) THE FIELD EQUATIONS

The cross-shelf and alongshelf momentum equations are

$$\frac{\partial u}{\partial t} + u\frac{\partial u}{\partial x} + w\frac{\partial u}{\partial z} - fv = -\frac{1}{\rho_0}\frac{\partial p}{\partial x} + \frac{\partial}{\partial z}\left(K_M\frac{\partial u}{\partial z}\right)$$

$$+ \frac{\partial}{\partial x}\left(A_M\frac{\partial u}{\partial x}\right) \qquad (1)$$

$$\frac{\partial v}{\partial t} + u\frac{\partial v}{\partial x} + w\frac{\partial v}{\partial z} + fu = \frac{\partial}{\partial z}\left(K_M\frac{\partial v}{\partial z}\right) + \frac{\partial}{\partial x}\left(A_M\frac{\partial v}{\partial x}\right). \qquad (2)$$

A right-handed "east coast" coordinate system is used, with x positive offshore, y positive northward, and z positive upward; K_M is the vertical eddy viscosity determined by the turbulence closure scheme. In all of the model runs, the Coriolis parameter $f = 10^{-4}$ s^{-1}, the gravitational acceleration $g = 9.80$ m s^{-2}, and the reference density $\rho_0 = 1020$ kg m^{-3}.

The density equation is

$$\frac{\partial \rho}{\partial t} + u\frac{\partial \rho}{\partial x} + w\frac{\partial \rho}{\partial z} = \frac{\partial}{\partial z}\left(K_H\frac{\partial \rho}{\partial z}\right) + \frac{\partial}{\partial x}\left(A_H\frac{\partial \rho}{\partial x}\right), \qquad (3)$$

where K_H is the vertical eddy diffusivity determined by the turbulence closure scheme. Although technically density is not a conserved quantity, a linear equation of state is assumed so that density is linearly proportional to temperature, which is conserved.

The water is assumed to be incompressible, so

$$\frac{\partial u}{\partial x} + \frac{\partial w}{\partial z} = 0. \qquad (4)$$

2) BOUNDARY CONDITIONS

The surface boundary condition is

$$K_M\frac{\partial(u, v)}{\partial z}\bigg|_{z=0} = (\tau^{sx}, \tau^{sy})\rho_0^{-1}, \qquad (5)$$

where τ^{sx} and τ^{sy} are the surface cross-shelf and alongshelf wind stress components, respectively. There is no buoyancy

flux through the surface.

The bottom boundary condition for momentum is a quadratic drag law:

$$K_M \frac{\partial(u, v)}{\partial z}\bigg|_{z=-H} = \rho_0 C_D (u_b^2 + v_b^2)^{1/2}(u_b, v_b), \quad (6)$$

where (u_b, v_b) represents the velocity in the bottom grid cell. Here C_D is a drag coefficient determined by

$$C_D = \kappa^2 \left(\ln \frac{\Delta z_b}{z_0} \right)^{-2}, \quad (7)$$

where $\kappa = 0.4$ is von Kármán's constant, Δz_b is half the vertical grid spacing at the bottom, and $z_0 = 10^{-2}$ m is the bottom roughness scale. Due to variation in the grid spacing as a function of the water depth, C_D varies in the base case from approximately 4.8×10^{-2} in 5 m of water to 6.9×10^{-3} in 55 m of water. There is no buoyancy flux through the bottom.

At the coastal wall, the boundary condition for the along-channel velocity is free-slip, and there is no cross-channel flow or buoyancy flux.
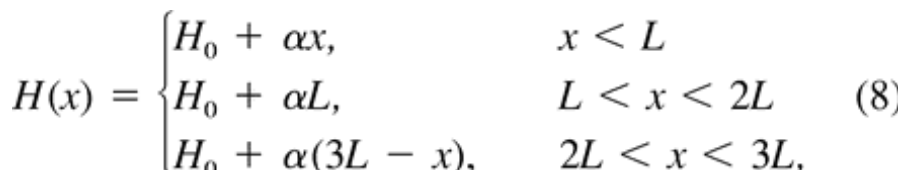
3) SPATIAL AND TEMPORAL GRIDS

POM is a sigma-level model, meaning that the vertical grid resolution is proportional to the water depth. In the base case, the depth varies from 5 m at the coast to 55 m in the middle of the channel (in a steep-slope run with $\alpha = 0.005$, the maximum depth is 255 m). With 40 sigma levels, the vertical resolution varies from approximately 0.13 m in shallow water to 1.4 m in the deepest portion of the domain (4.1 m in the steep-slope case). The vertical spacing near the surface and bottom is slightly smaller to resolve the boundary layers.

The horizontal grid size varies in proportion to the square root of the local depth, maintaining numerical stability while providing high resolution in shallower water. The horizontal resolution varies from approximately 150 m in the shallowest portion of the domain to approximately 450 m in the deepest portion. In the base case there are 339 grid cells in the horizontal; this number varies from 175 for the steep-slope case to 562 for the shallow-slope case.

The model utilizes a split time step, with an external time step ($\Delta t_E = 10$ s) to resolve the barotropic mode and an internal time step ($\Delta t_I = 150$ s) to resolve the baroclinic portion of the solution. Halving the time steps and halving both the time steps and the spatial grid resolution made no qualitative or significant quantitative change in the response.

b. Configuration of the base case model run

Three components are varied in the two-dimensional model runs: the bathymetry, the initial stratification, and the wind forcing (the initial condition is at rest). Simple forms are used so that these three components can be described with as few parameters as possible, thereby simplifying the analysis (Fig. 1 ⊙▬). The "base case" parameters described in this section are motivated by the observations made during the CoOP Inner Shelf Study (Austin and Lentz 1999; Austin 1998). The dependence of the model response on the wind forcing, stratification, and bathymetry are considered by varying these parameters.

1) BATHYMETRY

The model domain is a symmetric channel with bathymetry $H(x)$ given by

$$H(x) = \begin{cases} H_0 + \alpha x, & x < L \\ H_0 + \alpha L, & L < x < 2L \\ H_0 + \alpha(3L - x), & 2L < x < 3L, \end{cases} \quad (8)$$

where H_0 is the water depth at the coastal boundary, α is bottom slope, and L is the width of the sloped portion of the

shelf. In all of the model runs $L = 50$ km. Test runs (not presented here) showed doubling L did not qualitatively affect the response over the sloped shelf, suggesting that the channel was sufficiently wide that the opposite sides of the domain do not influence each other. In the base case, $H_0 = 5$ m and $\alpha = 10^{-3}$. The slope is approximately consistent with the bathymetry observed over the northeastern North Carolina inner shelf within 20 km of the coast, where the cross-shelf bottom slope was on the order of 10^{-3}, with significant variation on shorter spatial scales. An advantage of the symmetric configuration is that the downwelling and upwelling cases are solved simultaneously on opposite sides of the channel.

2) STRATIFICATION

The initial stratification consists of well-mixed surface and bottom layers with a continuously stratified pycnocline in between. The initial density as a function of depth is

$$\rho(z) = \begin{cases} \rho_0, & z > -Z_0 \\ \rho_0 + \Delta\rho\dfrac{(-Z_0 - z)}{\Delta Z}, & -Z_0 < z < -Z_0 - \Delta Z \\ \rho_0 + \Delta\rho, & -Z_0 - \Delta Z > z. \end{cases} \quad (9)$$

The variable parameters that determine the stratification are Z_0, the initial thickness of the surface mixed layer; $\Delta\rho$, the density change across the pycnocline; and ΔZ, the thickness of the pycnocline. The typical stratification observed during August 1994 at the CoOp Inner Shelf Study site was a strong pycnocline centered at approximately 10-m depth. The base case parameters are therefore: $Z_0 = 8$ m, $\Delta Z = 4$ m, and $\Delta\rho = 2$ kg m^{-3} (Fig. 1 ⬤▬).

3) WIND FORCING

The base case surface forcing consisted of alongshelf wind stress τ^{SFC}, uniform across-channel, ramped up over an inertial period, and left on for the duration of the model run (Fig. 1b ⬤▬). The wind stress is defined as

$$\tau^{SFC}(t) = \begin{cases} \tau^S\dfrac{ft}{2\pi}, & t < \dfrac{2\pi}{f} \\ \tau^S, & t > \dfrac{2\pi}{f}. \end{cases} \quad (10)$$

The ramp-up length was chosen to quell inertial energy. In the base case, $\tau^S = 0.1$ N m^{-2}, roughly equivalent to a wind speed of about 8 m s^{-1} at 10 m above the sea surface (Fairall et al. 1996). Wind events during the CoOP Inner Shelf Study typically lasted a couple of days (Austin and Lentz 1999). To investigate the response to the cessation of the wind, the wind forcing is ramped down after five inertial periods in several model runs and the subsequent relaxation is observed for four inertial periods.

Different model runs will be referred to by the parameter that has been changed and by how much, relative to the base case (BC). For instance, a model run identical to the BC except that the wind stress is twice as strong is called $2\tau^S$. A model run with no stratification, referred to as NEUT, is used as a control case to study the role of stratification.

c. Nondimensionalizations

The dynamics of the shelf are fundamentally different inshore and offshore of the upwelling front, and this makes nondimensionalization of the problem difficult. However, nondimensionalizing some of the variables aids in the interpretation of the results. In the rest of the paper, nonprimed variables are dimensional and primed variables are dimensionless. The primes will be retained throughout the paper since not all variables are nondimensionalized.

Time is scaled by the inertial period (17.5 h)

$$t' = \frac{f}{2\pi}t. \qquad (11)$$

No simple cross-shelf or vertical length scales that characterize the response were found. The internal Rossby radius of deformation (5 km in the base case) does not characterize the offshore location of the front. However, the internal Rossby radius characterizes the width of the front in the transient case in which the front comes into equilibrium with an alongshore jet, as in the classic Rossby adjustment problem.

The density anomaly $\rho - \rho_0$ is scaled by the initial density difference $\Delta\rho$

$$\rho' = \frac{\rho - \rho_0}{\Delta\rho}, \qquad (12)$$

where ρ_0 is the density of the water initially in the surface mixed layer and hence the lightest water in the system. Therefore, initially $\rho' = 0$ at the surface and $\rho' = 1$ in the lower layer.

The internal stress is scaled by the applied wind stress

$$\tau' = \frac{\tau}{|\tau^S|}. \qquad (13)$$

Thus, τ' ranges from 1 at the surface during the wind forcing to 0 in the interior. The value of the stress throughout the water column indicates whether the surface and bottom layers are in "direct contact" through the stress divergence field [i.e., Lentz's (1995) inner shelf] or whether there is an inviscid interior and the bottom boundary layer is driven entirely by the cross-shelf pressure gradient (i.e., the midshelf).

Finally, the cross-shelf streamfunction Ψ is defined as $\Psi_z = -u$, $\Psi(z = 0) = 0$, and is scaled by the Ekman transport

$$\Psi' = \left(\frac{\tau^S}{\rho_0 f}\right)^{-1}\Psi. \qquad (14)$$

Thus, if there is no stress in the interior and a full Ekman layer develops, then $\|\Psi'\| \approx 1$ in the interior.

3. Base-case response

In this section, we consider the two-dimensional response of an idealized stratified coastal ocean to constant upwelling- and downwelling-favorable wind stresses. Descriptions of the base case upwelling and downwelling scenarios are presented, followed by comparisons and scalings of key elements of the response, such as the size of the inner shelf and the alongshore geostrophic transport associated with the upwelling or downwelling jet.

a. Upwelling

The response to upwelling favorable winds (Fig. 2 ⊙➡) resembles the classic coastal upwelling circulation (Smith 1995). After one inertial period ($t' = 1$), the wind stress, which has reached full intensity, accelerates a surface-intensified alongshelf flow, which in turn accelerates an offshore flow due to the Coriolis force, resulting in the formation of a surface Ekman layer. The offshore Ekman transport in the surface boundary layer sets up a cross-shelf pressure gradient that drives an onshore return flow that is evenly distributed throughout the water column. A bottom mixed layer has formed where the pycnocline intersects the bottom, and the isopycnals have begun to move onshore. The alongshelf velocity is surface intensified and strongest near the coast. After two inertial periods ($t' = 2$), divergence in the wind-driven offshore transport near the coast forces upwelling that causes the pycnocline to intersect the surface, forming an upwelling front about 12 km offshore. A region of less dense water is left near the coast, separated from the upwelling front by a bulge of denser upwelled water. The cross-shelf flow is well developed offshore of the front with the surface-layer offshore transport and the lower-layer onshore transport equal to the classical Ekman transport $\tau^s \rho_0^{-1} f^{-1}$ ($\Psi' \approx 1$ in the interior). Inshore of the front the cross-shelf flow decreases toward the coast. This divergence in the cross-shelf transport leads to the large vertical velocities. The alongshore flow increases throughout the domain and a jet develops at the front, with maximum velocities of ~ 0.5 m s^{-1}. After three inertial periods ($t' = 3$) the upwelling front and the associated alongshelf jet have moved farther offshore (20 km), expanding the inner shelf region. The stratification over the inner shelf has weakened causing a reduction

of the cross-shelf circulation. Consequently, most of the cross-shelf transport divergence, and hence the upwelling, occurs near the upwelling front. However, weak stratification and a weak cross-shelf circulation do persist over the inner shelf. At longer times, the front and associated features continue to move offshore and the inner shelf region continues to expand. Otherwise the density and flow fields remain essentially the same.

b. Downwelling

The initial response to downwelling-favorable winds is essentially the same as the initial response to upwelling-favorable winds except the cross-shelf and alongshelf flows are in the opposite direction (cf Figs. 2 ⊙ and 3 ⊙, $t' = 1$). However, at longer times there are notable differences in the response. Downwelling-favorable winds drive an onshore Ekman transport in the surface boundary layer that results in a vertically uniform offshore flow (Fig. 3 ⊙, $t' = 1$). The offshore flow displaces the pycnocline by deepening it across the shelf with greater deepening closer to shore. The alongshelf flow is surface intensified and varies little across the shelf. After two inertial periods ($t' = 2$), the offshore flow is concentrated near the bottom, indicating the formation of a bottom boundary layer. The bottom boundary layer transport deflects and steepens the downwelling front, producing a region of strong cross-shelf density gradient. Just onshore of the downwelling front is a region of large cross-shelf transport divergence and large downward vertical velocities. Farther onshore, on the inner shelf, cross-shelf velocities are very small. By $t' = 2$, a strong surface-intensified jet has formed in the vicinity of the downwelling front. Velocities in the jet near the surface approach 0.5 m s^{-1}, and increase in time as the depth of the downwelling front increases. Inshore of the jet the alongshelf velocities are much weaker, and the flow is less sheared, with velocities throughout the region on the order of 0.2 m s^{-1}. There is little change in the cross-shelf and alongshelf circulation after two inertial periods except that the location of the downwelling front, the associated jet, and the cross-shelf flow divergence move offshore.

c. Cross-shelf transport

An important component of the upwelling and downwelling responses is the development of the cross-shelf circulation, which redistributes the density field. The maximum value of the streamfunction $\|\Psi'\|$ as a function of cross-shelf location is a proxy for the cross-shelf transport (Fig. 4 ⊙), and is calculated by integrating the cross-shelf velocity above the first zero crossing, similar to Allen et al. (1995). Initially ($t' = 1$) the spinup across the shelf results in increasing cross-shelf circulation offshore during both upwelling and downwelling. At later times ($t' > 1$) there is a rapid change in transport in the vicinity of the upwelling or downwelling front. Offshore of the front, $\|\Psi'\| \approx 1$ because the stress in the middle of the water column is approximately zero due to the strong vertical stratification (Figs. 2 ⊙ and 3 ⊙). In the case of downwelling, part of the increase in the cross-shelf transport occurs offshore of the front where the pycnocline tilts down toward the coast. Over the inner shelf, inshore of the front, the stratification is not strong enough to completely suppress vertical mixing, and τ' does not approach zero anywhere in the water column. Consequently the wind-driven cross-shelf transport is small. However, for upwelling the cross-shelf circulation on the inner shelf is stronger than for the equivalent case with no stratification (Fig. 4 ⊙, dashed curve). For downwelling, the cross-shelf circulation is slightly weaker than the equivalent case with no stratification, that is, weaker than for upwelling.

d. Depth-averaged alongshore momentum balance

For both upwelling and downwelling the bottom stress tends to balance the surface stress both onshore and offshore of the front (Fig. 5 ⊙) after an initial adjustment period. Over the inner shelf, the stress is nearly constant throughout the water column (Figs. 2 ⊙ and 3 ⊙). Offshore of the front, the stresses are concentrated near the surface and bottom and are small in the interior. The transport in the surface and bottom Ekman layers have equal magnitudes, but opposite directions, and hence the stresses are the same. For upwelling there is not a significant variation in this balance in the vicinity of the front. However, for downwelling there is a substantial variation near the front. At the front and just offshore of the front (where the isopycnals are warped downward) the acceleration term is significant since the alongshore velocity is adjusting to the shear supplied by the horizontal density gradients present in these regions. In a narrow region just onshore of the front, the maximum bottom stress is over twice as large as the surface stress because the strong vertical stratification of the pycnocline has been advected offshore, leaving the high-momentum water on the inshore edge of the jet "exposed" to the bottom. Thus the large bottom stress in this region decelerates the alongshelf flow. A simple scaling of the dominant momentum balance in this region:

$$\upsilon_t \approx (K_M \upsilon_z)_z \quad (15)$$

yields a scaling for the time it takes to dissipate this momentum and reach the balance observed on the rest of the inner shelf:

$$T_{adj} \approx \frac{H^2}{\|K_M\|},\qquad(16)$$

where H is the local water depth and $\|K_M\|$ is a representative eddy viscosity. For $t' = 3$ in Fig. 5 O=, $H \approx 25$ m. Using $\|K_M\| = 10^{-2}\ \mathrm{m^2\ s^{-1}}$ (Fig. 6 O=), this yields $T_{adj} = 0.7$ days. Multiplying this by the offshore speed of the front, roughly $0.06\ \mathrm{m\ s^{-1}}$, yields 4 km, consistent with the observed width of the adjustment region (Fig. 5 O=).

e. Frontal speed and displacement

The displacement of the front during upwelling and downwelling determines the width of the inner shelf. The rate at which the front moves offshore is different for upwelling and downwelling. The surface and bottom temperature fields from the upwelling and downwelling cases (Fig. 7 O=) suggest that for upwelling the offshore position of the front is a linear function of time t, while for downwelling the position increases as roughly $(t)^{1/2}$ (the scales of the model fits shown in this figure are those derived later in this paper). The difference is due the geometry as discussed below. In Allen and Newberger (1996), this dependence is evident in the downwelling case, but is less clear in the upwelling case of Allen et al. (1995), largely because the surface front is not as well defined in the continuously stratified case considered there. Surface mixing, in this case, plays a significant role in determining the surface density distribution, obscuring the position of the surface front.

To first order, the rate of the offshore displacement of the upwelling front is simply the Ekman transport divided by the surface Ekman layer depth δ_E; that is, the velocity of the front is hypothesized to be

$$u_F = \frac{\tau^S}{\rho_0 f \delta_E},\qquad(17)$$

where u_F is the vertically averaged velocity in the surface Ekman layer. This corresponds to an offshore displacement of

$$\Delta X = t\frac{\tau^S}{\rho_0 f \delta_E},\qquad(18)$$

where t is the duration of the wind event. This equation is only approximate in that it does not take into account the time it takes the front to reach the surface or the location at which it does so. This issue is clearly evident in Fig. 7 O=, where a surface upwelling front does not start to form until after 1 inertial period. The velocity is not vertically uniform in the surface boundary layer, as the offshore velocity at the surface is somewhat greater than that below. This leads to a weak overturning that keeps the front steep. This behavior has been observed in other numerical models (Chen and Wang 1990; Hamilton and Rattray 1978). Based on the initial conditions, a reasonable estimate of the effective Ekman depth for the case of a strong, shallow pycnocline considered here is $\delta_E \approx Z_0 + \Delta Z/2$, where Z_0 is the initial depth of the surface mixed layer. The addition of a portion of the pycnocline ($\Delta Z/2$) is similar to the "transition layer" discussed in Lentz (1992). This estimate of δ_E assumes the stratification in the pycnocline is strong enough to inhibit vertical mixing and deepening of the surface mixed layer and is inaccurate if the mixed layer deepens substantially over the forcing period. Estimates of mixed layer deepening are discussed in appendix A. Taking these estimates of mixed layer deepening into account qualitatively improves the displacement estimates. The Ekman layer thickness estimate may also be invalid if the initial mixed layer depth is greater than the neutral Ekman layer depth $\kappa u_*/f$, where $u_* = (\tau^S \rho^{-1})^{1/2}$, in which case $\delta_E \approx \kappa u_*/f$. However, this is not the case for any of the scenarios tested here.

A comparison (Fig. 8A O=) of measured displacement between 2 and 8 inertial periods with this scaling (this interval is used to avoid the spinup period in which the front reaches the surface) shows good agreement for small displacements, but increasingly poor agreements as the scaled displacement increases. This disagreement is largely due to mixed layer deepening during the model run. It is interesting to note that conditions that should lead to relatively large offshore displacement, such as high wind stresses or shallow surface mixed layers, are also those that are most susceptible to mixed layer deepening.

In contrast to the upwelling case, during downwelling the front is initially driven offshore by the barotropic response, until the bottom Ekman layer is spun up, at which point it dominates the displacement of the front. The initial barotropic response is more important during downwelling than upwelling because the bottom Ekman layer takes longer to spin up than the surface Ekman layer (see Figs. 2 O= and 3 O=). The details of the transport mechanisms are considered in more detail in Dever (1997) and Austin (1998).

The initial vertically uniform offshore flow (Fig. 3 ⊙, Ψ, $t' = 1$) over a sloped bottom results in vertical velocities, which are zero at the surface and largest at the bottom. These vertical velocities cause the largest downward displacements of the pycnocline near the bottom (close to shore) and the smallest vertical displacements near the surface (farther offshore). This results in the pycnocline sloping downward towards the shore and being displaced offshore (see density contours Fig. 3 ⊙ $t' = 2$). Assuming that initially the offshore transport in the interior equals the onshore surface Ekman transport ($U^S = \tau/\rho f$), the approximate deflection of the pycnocline due to the barotropic response can be estimated. If the horizontal velocity field is

$$u_{\mathrm{BARO}}(x) = -\frac{U^S}{H(x)}, \qquad (19)$$

continuity ($u_x + w_z = 0$) can be used to estimate the vertical velocity field w:

$$w_{\mathrm{BARO}}(x, z) = \frac{\alpha U^S z}{H(x)}. \qquad (20)$$

To determine the displacement of isopycnals, define a coordinate system $x' = H_0 \alpha^{-1} + x$ so that $H = \alpha x'$. Then, writing (19) in terms of cross-shelf displacements

$$\frac{dx'}{dt} = -\frac{U^S}{\alpha x'} \qquad (21)$$

and integrating in time yields

$$(x'^2 - X_0^2) = 2\alpha^{-1} \int_0^t U^S \, dt. \qquad (22)$$

The displacement of the location of the intersection of the pycnocline with the bottom can now be written as a function of time:

$$x_{\mathrm{BARO}}(t) = \sqrt{\int_0^t \frac{2U^S}{\alpha} \, dt + X_0^2}, \qquad (23)$$

where X_0 is the initial position of the front.

For times long compared to the frictional timescale the offshore displacement of the front is dominated by the transport in the bottom Ekman layer and the barotropic response can be neglected. In this case, the bottom Ekman transport equals the surface Ekman transport (U^S). The bottom Ekman transport pushes slightly lighter water from just onshore of the downwelling front under the front, resulting in steepening (Fig. 3 ⊙, ρ, $t' = 2, 3$). The steepening behavior is similar to that observed in upwelling fronts in other modeling studies (Hamilton and Rattray 1978; Chen and Wang 1990). By setting the surface volume transport equal to the volume displaced by the downwelling front, the location of the front can be estimated:

$$\frac{1}{2}(\Delta x_{\mathrm{EK}})(\alpha \Delta x_{\mathrm{EK}}) = \int_0^t U^S \, dt, \qquad (24)$$

where Δx_{Ek} is the displacement of the downwelling front due to this mechanism. This can be rearranged to yield:

$$x_{\mathrm{EK}}(t) = X_0 + \sqrt{\int_0^t \frac{2U^S}{\alpha} \, dt}. \qquad (25)$$

The actual displacement is a combination of the initial shelfwide deepening of the pycnocline by the barotropic response,

and then the steepening of the front by the bottom Ekman layer. However, for a constant wind stress, the displacement scales in both mechanisms as approximately:

$$\Delta X \approx \sqrt{\frac{2\tau^S t}{\rho_0 f \alpha}}, \qquad (26)$$

where t is the time since onset of the wind. Variations in the frontal displacement due to changes in τ^S and α are in good agreement with this scaling (Fig. 8b ⊙), except at very small values of α, in which the downwelling front is smeared out, making the displacement difficult to measure. The success of this scaling suggests that the initial density structure plays little role in determining the offshore propagation of the pycnocline and, in fact, model runs where stratification parameters are varied, including runs with constant stratification, show little variation in pycnocline displacement. It is clear from Fig. 8 ⊙ that the cross-shelf frontal displacement scale for downwelling is typically less than that for upwelling. Thus, though the surface Ekman transport is the same for both upwelling and downwelling, the frontal displacement has significantly different dependences. For upwelling the offshore displacement of the front is a linear function of time because δ_E is roughly constant. For downwelling, δ_E (or the depth for the barotropic response) increases with time as the front moves into deeper water (see Fig. 3 ⊙), so for a constant U^S the rate of offshore displacement must decrease with time.

f. The relaxation response: Alongshelf geostrophic transport

Alongshelf transport in the jet associated with the upwelling or downwelling front also plays an important role in shelf circulation. Alongshelf variation in the transport gives rise to alongshore divergences, which may play an important role in setting up alongshore pressure gradients likely responsible for the observed (but not modeled) relaxation response. To understand what gives rise to these divergences, we must first understand what sets the scale of the transport for the local response.

In both the upwelling and downwelling case, the geostrophic transport in the jet is calculated from the local density field assuming no flow at the bottom. In the case where the alongshore wind is shut off, the system responds by dissipating alongshore momentum through bottom friction until the bottom velocity is zero; however, thermal wind shear above the bottom allows momentum to be "trapped" in the upper portion of the water column, in geostrophic balance with the density field. From a model run that has had the wind shut off and allowed to come to equilibrium (Fig. 9 ⊙), it is clear that for both the upwelling and downwelling the system does relax to a geostrophic balance. In the case of upwelling, the cross-shelf density gradients are in the upper portion of the water column (Fig. 10a ⊙). Whereas, in downwelling, the cross-shelf density gradients are concentrated near the bottom (Fig. 10b ⊙). An important consequence of this difference is that the transport in the downwelling jet grows with offshore displacement, whereas it is constant in the upwelling case.

An estimate of the geostrophic transport in the upwelling jet, when the wind is turned off after a wind stress of duration Δt, is

$$V_{trans} = \frac{g \Delta \rho (Z_0 + \Delta Z/2)^2}{2\rho_0 f}. \qquad (27)$$

Thus, in the absence of substantial mixing across the pycnocline, the geostrophic transport in the jet after the wind is turned off is independent of the strength or duration of the forcing, as long as it is of sufficient duration to bring the pycnocline to the surface. This scale estimate of the geostrophic transport is in good agreement with the observed transport from the numerical model runs (Figs. 11a ⊙ and 11c ⊙). The scalings for weak forcing ($\tau^S/5$) and deep initial surface layer ($5Z_0$) overestimate the jet transport because in these two cases the wind stress event is insufficient to fully outcrop the pycnocline over the duration of the run. Taking into account the deepening of the pycnocline due to mixing only slightly improves the estimates since its effects at least partially cancel out: Mixing simultaneously deepens the mixed layer (which increases jet transport) and decreases the density difference across the front (which decreases transport).

In downwelling, the geostrophic transport is distributed over a greater depth as the jet moves farther offshore (Fig. 10b ⊙). The alongshelf, geostrophic velocity in the jet is

$$v_{jet} = \begin{cases} \dfrac{g}{\rho_0 f} \dfrac{\Delta\rho}{D}(H(X_F) - Z_0), & z > -Z_0 \\[3mm] \dfrac{g}{\rho_0 f} \dfrac{\Delta\rho}{D}(z + H(X_F)), & -H(X_F) < z < -z_0, \end{cases}$$

$$(28)$$

where $H(X_F)$ is the water depth at the location of the front, X_F. Integrating v_{jet} vertically and multiplying by the width of the jet D results in an estimated total jet transport:

$$V_{trans} = \frac{g\delta\rho}{2\rho_0 f}(H(X_F)^2 - Z_0^2).$$

$$(29)$$

This is initially difficult to interpret because the time dependence is buried in the X_F term. However, the frontal depth $H(X_F)$ can be estimated using the displacement scaling (25). The variation in bottom depth over the width of the jet is ignored. The density difference and mixed layer depth can be approximated, to first order, as $\delta\rho = \Delta\rho$ and $\delta_E = Z_0$, yielding

$$V_{trans} = \frac{g\delta\rho}{2\rho_0 f}2U^S\alpha t.$$

$$(30)$$

The scaling underestimates the jet transport by nearly a factor of 2, but the parameter dependence is good (Fig. 11b 🔵). The difference is presumably due to inappropriate choices of $\delta\rho$ and Z_S due to the effects of entrainment. During downwelling, reducing the density difference and deepening the mixed layer both reduce the total transport, causing the simple scaling to significantly overestimate the transport. In this case, the inclusion of the mixing scaling significantly improves the estimate (Fig. 11b 🔵). The magnitude of the jet in the downwelling case is much larger than in the upwelling case. For instance, the measured (modeled) transport in the base case for upwelling is approximately 2×10^4 m^3 s^{-1}, whereas for downwelling it is nearly 6×10^4 m^3 s^{-1}.

g. The inner shelf

The inner shelf, inshore of the upwelling or downwelling front, is a distinct region with characteristics determined by the interplay between stratification, vertical mixing, and the cross-shelf circulation. In this region, the stress magnitude is significant relative to the surface stress throughout the entire water column; that is, the surface and bottom Ekman layers interact directly. In the absence of any initial stratification, the response to upwelling and downwelling favorable winds is essentially the same except that the circulation patterns are reversed. However, in the stratified case, the inner shelf response to upwelling and downwelling favorable winds is different due to the cross-shelf advection of density.

During upwelling, the inner shelf is characterized by weak vertical stratification and weak cross-shelf circulation (Fig. 2 🔵). The weak vertical stratification is maintained by the onshore flow of denser water near the bottom and offshore flow of lighter water near the surface. The weak vertical stratification inhibits vertical mixing. Eddy viscosities, K_M (Fig. 6a 🔵), from two sites on the inner shelf are smaller at mid depth than for the unstratified (neutral) model run. (The site 20 km offshore, is offshore of the upwelling front, and hence the dip in the eddy viscosity profile halfway through the water column is due to the strong vertical stratification of the pycnocline.) The reduced eddy viscosities at mid depth allow a small stress divergence that drives a weak cross-shelf circulation, which is stronger (Fig. 4a 🔵) than the cross-shelf circulation in the neutral case (dashed curve). In the case of vertically uniform initial stratification the inner shelf cross-shelf circulation and stratification are stronger because there is a continual source of denser water offshore (see section 4a below).

During downwelling, the inner shelf is unstratified and there is almost no cross-shelf circulation. The inner shelf is unstratified because of the very weak downwelling-favorable circulation. As near-surface water is advected onshore, slightly lighter water is advected offshore near the bottom, resulting in convective adjustment. The convective adjustment increases the eddy viscosity above what would be expected in the absence of stratification (Fig. 6b 🔵). This increases the Ekman depth and decreases the strength of the cross-shelf circulation (Fig. 4b 🔵). For the base case, the inner shelf cross-shelf circulation during upwelling is more than twice as strong as during downwelling. This asymmetry increases as the initial stratification is increased. For the neutral case (no initial stratification), the upwelling and downwelling cross-shelf transport magnitudes are identical.

There is a cross-shelf density gradient over the inner shelf during both upwelling and downwelling. During upwelling, light water near the coast is trapped when the bottom boundary layer forms, moves onshore, and domes the isopycnals so that they contact the surface offshore of the coast. Once the isopycnals have domed and separated from the main pycnocline, water moving onshore along the bottom mixes with light water moving offshore at the surface, resulting in local changes in the density field far slower than if advection acted alone. Thus, isopycnals on the inner shelf move much more slowly offshore than cross-shelf velocities in that region would suggest because of this advective–diffusive balance. As the water entering the region is always denser than the water leaving the region, the region must on average become denser, but over much longer timescales than the advective timescale.

During downwelling, the inner shelf structure is set up as the front moves offshore. The density at a given point is set by the density in the upper layer at the time the front passes that position, so for the inner shelf $\rho'(x) = \rho'_u[X_f^{-1}(x)]$, where $\rho_u(t)$ is the density in the upper layer and $X_f(t)$ is the location of the front. This is demonstrated for the base case in Fig. 12, which shows that the density difference across the inner shelf is nearly a third of the density difference across the pycnocline. Combining the rate of densification of the surface layer (appendix A) with the pycnocline displacement scale (26) allows the estimation of the dependence of the size of the cross-shelf density gradient on the inner shelf on the model parameters. The scaling itself is quite involved and is covered in Austin (1998). The most important aspect of this process is that the density gradient will always be of the same sign; the lightest water will always be found closest to the shore. Therefore, the inner shelf during downwelling will always be a region of very weak cross-shelf circulation. For strong forcing, when local mixing may be more important than advection for determining the eventual cross-shelf density profile the lightest water is still found near the coast. As the actual shelf response is going to be some combination of advection and mixing, the orientation of this gradient is not sensitive to the strength of the mixing event, and the lightest water is always found onshore. However, the density gradients produced by this process are typically weak, and therefore processes not considered here (such as surface heating or cooling, or the influx of freshwater) may act to modify this gradient.

4. Discussion

a. Continuous stratification

We briefly consider the formation of the inner shelf in the scenario where the water is continuously stratified. By extending the stratification throughout the water column, the upwelling response is changed considerably but the downwelling response remains largely the same.

During upwelling (Fig. 13, first column), instead of the inner shelf being fed by a body of constant-density water as in the two-layered case considered in the previous section, there is a constant supply of increasingly denser water to the inner shelf. In the case of constant stratification, the inner shelf density and cross-shelf circulation are quite different from the two-layer case (Fig. 2, $t' = 3$). The constant source of buoyancy keeps the inner shelf more strongly stratified, which allows more of the cross-shelf circulation to extend onshore of the upwelling front. As a result, much of the divergence in the cross-shelf flow, and hence the upwelling, occurs over the inner shelf. The specific character of the nearshore circulation and the cross-shelf divergence in the Ekman layer depends on the relative values of the stratification and the slope. Specifically, large Burger number flows (i.e., steep slopes or strong stratification) tend to lead to a shutdown in the bottom boundary layer (MacCready and Rhines 1993), which affects the character of the return flow and, hence, the inner shelf. However, this is beyond the scope of this paper.

In contrast, during downwelling (Fig. 13, second column), as a surface mixed layer is quickly formed, water of roughly constant density is driven onshore, forming a downwelling front that moves offshore much like in the pycnocline case (Fig. 3, $t' = 3$). For a wide range of parameters, this same inner shelf structure forms during downwelling. The formation of an inner shelf region during downwelling on a stratified shelf may serve as a potential explanation of drifter behavior observed by Barth and Smith (1998). Drifters released during several winter seasons off the coast of Oregon (Fig. 14 shows two drifter paths and the alongshore winds from the 1994–95 season) all tended to move onshore during downwelling favorable wind events (the prevalent forcing during the winter). The drifters would approach the coast, then rapidly be advected northward, maintaining a roughly constant distance from the coast. It appears that once drifters pass over the cross-shelf position of the downwelling front, the cross-shelf velocities they are subjected to are very small, and they maintain their cross-shelf displacement over alongshore distances of several hundred kilometers, even in the presence of significant downwelling-favorable winds. A more complete analysis of the behavior of drifter motion over the Oregon–Washington shelf during downwelling-favorable winds is forthcoming (Austin and Barth 2002, manuscript submitted to J. Phys. Oceanogr.).

b. Cross-shelf particle transport

A major objective of the CoOP Inner Shelf Study (Butman 1994) was to develop and test hypotheses concerning the cross-shelf transport of planktonic larvae. To establish a "baseline" hypothesis concerning cross-shelf transport on a two-layered shelf, model runs that included a passive tracer release were conducted. Two separate configurations were tested,

both intent on exploring potential wind-driven processes that bring larvae to or away from the coastal boundary. In the first experiment, a patch of uniform concentration tracer was placed in the nearest 2 km to shore (Figs. 15 ⬤ and 16 ⬤, column 2). In the second experiment, a patch of uniform concentration tracer is placed below the pycnocline for upwelling and above the pycnocline for downwelling, between 20 km and 22 km offshore (Figs. 15 ⬤ and 16 ⬤, column 1). Passive tracers started offshore above the pycnocline during upwelling or below the pycnocline during downwelling simply moved offshore at approximately the speed of the front (not shown). Results are similar for upwelling and downwelling.

In the case in which the tracer starts at the coast, it does not escape the nearshore region to be transported offshore. In the upwelling case the tracer patch is trapped inside the location of the initial pycnocline shoaling and is subject to the same advective–diffusive balance as the density field. Consequently it does not spread offshore very rapidly. In the case of downwelling, the inner-shelf cross-shelf circulation is very weak and again the patch does not spread very rapidly.

In the downwelling case where the tracer is above the pycnocline (Fig. 16 ⬤, column 1), the tracer moves onshore until it passes over the downwelling front. After the downwelling front passes, the tracer mixes vertically to span the water column and its cross-shelf position remains fixed. Subsequently, the maximum concentration slowly decreases as the tracer is horizontally diffused away. In the upwelling case where the tracer starts below the pycnocline (Fig. 15 ⬤, column 1), the tracer exhibits a similar response. In this case, the tracer is advected onshore until the surface upwelling front passes over the tracer patch. At this point, the tracer enters the region in which the vertical mixing is strong from the surface to the bottom, and is immediately mixed throughout the water column. The tracer is then subject to an advective–diffusive balance, and its cross-shelf position remains fixed. The maximum concentration at this point slowly decreases as the tracer is horizontally diffused away.

The upwelling case (Fig. 15 ⬤, column 1) is similar to steady shear-induced dispersion, commonly observed in estuaries. It can be shown (Fischer 1979) that given a vertically uniform vertical diffusivity K_H, the effective horizontal diffusion rate K_{horiz} is

$$K_{horiz} \approx \frac{u_0^2 H^2}{120 K_H},\qquad (31)$$

where u_0 is the cross-shelf velocity scale and H the depth. The cross-shelf velocity scale u_0 on the inner shelf is taken from Lentz (1995, his Fig. 3), and for shallow water is approximated by

$$u_0 \approx 0.25 \frac{\tau^s}{\rho_0} \delta^{-1} f^{-1},$$

where $\delta = \kappa u_*/f$. The eddy diffusion term K_H can be approximated with $K_H \approx \kappa u_* z(1 + z/H)$ (based on Fig. 6 ⬤) and using the vertically averaged value of K_H for $\tilde{K}_H$ (i.e., $\tilde{K}_H \approx H^{-1} \int_{-H}^{0} K_H dz$), we get a scale for K_{horiz} on the inner shelf of

$$K_{horiz} \approx 0.003 \frac{H u_*}{\kappa^3},\qquad (32)$$

which for the base case ($u_* \approx 0.01$ m s^{-1}) in 20 m of water gives $K_{horiz} = 0.01$ m^2 s^{-1}, which for the timescales of interest does not represent significant horizontal diffusion ($L \sim (KT)^{1/2} \sim (0.01$ m^2 s^{-1} 3×10^5 s$)^{1/2} \sim 60$ m).

Passive tracer runs were made in two other cases: that of a continuously stratified shelf (as in Fig. 13 ⬤) and that of an unstratified shelf (the neutral case used in Figs. 4 ⬤ and 6 ⬤). Figure 17 ⬤ shows the tracer patch at $t' = 4$ for each of these scenarios, in which a patch of tracer was released 20 km offshore, at the surface in the downwelling case, and at the bottom in the upwelling case, as in Figs. 15 ⬤ and 16 ⬤.

In the neutral case, for both upwelling and downwelling (Figs. 17e,f ⬤), the tracer patch was quickly mixed throughout the water column, resulting in identical distributions, which stay fixed over time. In the continuously stratified case with upwelling winds (Fig. 17c ⬤), the tracer is initially transported offshore, and then is "smeared" over a wide region as much of it enters the surface layer and is transported offshore. Almost none of the tracer reaches the coastal boundary. However, the tracer moves considerably farther onshore than it does in the strong pycnocline case (Fig. 17a ⬤). During downwelling (Fig. 17d ⬤), the response of the tracer patch is almost identical to that in the strong pycnocline case (Fig. 17b ⬤), as expected.

These results suggest that two-dimensional wind-driven upwelling or downwelling is not sufficient, in itself, to provide transport to or from a coastal boundary on a strongly two-layered shelf such as that off of the east coast of the United States. This is not to say, of course, that such transport does not or cannot occur. However, this places a larger burden of explanation on investigators who have, in the past, attributed such transport to simple two-dimensional wind-driven upwelling or downwelling. It must be combined with one of several possible supplemental mechanisms. Two likely candidates are planktonic swimming behavior (notably, vertical migration behavior) and alongshelf variation. Vertical migration behavior could play a role if, for instance, plankton were for some reason likely to swim toward the bottom during upwelling. If the swimming was sufficiently strong to overcome the effects of vertical mixing, then the plankton would spend a disproportionate amount of time in the lower layer, and hence in water moving onshore. This may also work to the advantage of species who must remain near the coastal boundary for their survival; the "nonleaky" character of the inner shelf may help to keep some species near the coastal boundary.

5. Summary

Idealized numerical model studies of two-dimensional upwelling and downwelling on a strongly stratified (two-layered) shelf are used to understand various aspects of the formation and characteristics of the inner shelf. For the unstratified case, the response to upwelling- and downwelling-favorable winds is essentially the same except the direction of the circulation is reversed. However, with stratification there are notable differences in the characteristics of the upwelling and downwelling fronts and the inner shelf region inshore of the front. In upwelling, weak stratification is maintained over the inner shelf by the onshore flux of denser near-bottom water. This weak stratification suppresses vertical mixing, causing a small reduction in stress at mid depth that drives a weak cross-shelf circulation over the inner shelf. For constant stratification, as opposed to the two-layer case, the inner shelf stratification and cross-shelf circulation are stronger. In downwelling, the inner shelf becomes unstratified because the very weak cross-shelf circulation forces lighter water under denser driving convection, which enhances the vertical mixing. As a result the stress is nearly constant across the water column and the cross-shelf circulation is weaker than in the initially unstratified case. The downwelling response is essentially the same for the constant stratification and the two-layer cases. The width of the inner shelf increases as the upwelling or downwelling front continues to move offshore. For a constant wind stress the upwelling front moves offshore at roughly a constant rate. The offshore speed of the downwelling front scales as $(t)^{1/2}$ because the thickness of the lower layer increases as the front moves offshore over a sloping bottom. The geostrophic transport is larger in the case of downwelling relative to upwelling because the same geostrophic shear is near the bottom in downwelling as opposed to near the surface in upwelling. Deepening of the pycnocline due to wind-driven mixing may play a significant role in determining the quantitative aspects of these scalings. Finally, transport of a passive tracer across the inner shelf is relatively difficult due to the strong vertical mixing. This suggests that more sophisticated conceptual models may be necessary for understanding larval settlement processes that require larvae to migrate from the coast to points farther offshore and back.

REFERENCES

Allen J. S., and P. A. Newberger, 1996: Downwelling circulation on the Oregon continental shelf. Part I: Response to idealized forcing. *J. Phys. Oceanogr.*, **26**, 2011–2035. Find this article online

Allen J. S., and J. Federiuk, 1995: Upwelling circulation on the Oregon continental shelf. Part I: Response to idealized forcing. *J. Phys. Oceanogr.*, **25**, 1843–1866. Find this article online

Austin J. A., 1998: Wind-driven circulation on a shallow, stratified shelf. Ph.D. thesis, Massachusetts Institute of Technology–Woods Hole Oceanographic Institution, MIT/WHOI 98-19, 243 pp.

Austin J. A., and S. J. Lentz, 1999: The relationship between synoptic weather systems and meteorological forcing on the North Carolina Inner Shelf. *J. Geophys. Res.*, **104**, 18159–18185. Find this article online

Barth J. A., and R. L. Smith, 1998: Separation of a coastal upwelling jet at Cape Blanco, Oregon, USA. *Benguela Dynamics: Impacts of Variability on Shelf-Sea Environments and their Living Resources.* S. C. Pillar, et al., Eds., *S. Afr. J. Mar. Sci.*, **19**, 5–14. Find this article online

Blumberg A. F., and G. L. Mellor, 1987: A description of a three-dimensional coastal ocean circulation model. *Three Dimensional Coastal Ocean Models,* N. Heaps, Ed., Coastal and Estuarine Science Series, Vol. 4, Amer. Geophys. Union, 1–16.

Butman C. A., 1994: CoOP: Coastal Ocean Processes Study, interdisciplinary approach, new technology to determine coupled biological, physical, geological processes affecting larval transport on inner shelf. *Sea Technol.,* **35**, 44–49. Find this article online

Chen D., and D.-P. Wang, 1990: Simulating the time-variable coastal upwelling during CODE-2. *J. Mar. Res.,* **48**, 335–358. Find this article online

Dever E. P., 1997: Wind-forced cross-shelf circulation on the northern California shelf. *J. Phys. Oceanogr.,* **27**, 1566–1580. Find this article online

Ekman V. W., 1905: On the influence of the earth's rotation on ocean-currents. *Arkiv Math., Astro. Fys.,* **2**, 1–53. Find this article online

Fairall C. W., E. F. Bradley, D. P. Rogers, J. B. Edson, and G. S. Young, 1996: Bulk parameterization of air–sea fluxes for Tropical Ocean–Global Atmospheric Coupled-Ocean Atmospheric Response Experiment. *J. Geophys. Res.,* **101**, 3747–3764. Find this article online

Fischer H., 1979: *Mixing in Inland and Coastal Waters.* Academic Press, 483 pp.

Foo E.-C., 1981: A two-dimensional diabatic isopycnal model—Simulating the coastal upwelling front. *J. Phys. Oceanogr.,* **11**, 604–626. Find this article online

Galperin B., L. H. Kantha, S. Hassid, and A. Rosati, 1988: A quasi-equilibrium turbulent energy model for geophysical flows. *J. Atmos. Sci.,* **45**, 55–62. Find this article online

Hamilton P., and M. Rattray Jr., 1978: A numerical model of the depth-dependent, wind-driven upwelling circulation on a continental shelf. *J. Phys. Oceanogr.,* **8**, 437–457. Find this article online

Kundu P. K., 1984: Numerical calculations of coastal flow with turbulent dynamics. *Deep-Sea Res.,* **31**, 39–60. Find this article online

Lentz S. J., 1992: The surface boundary layer in coastal upwelling systems. *J. Phys. Oceanogr.,* **22**, 1517–1539. Find this article online

Lentz S. J., 1995: Sensitivity of the inner-shelf circulation to the form of the eddy viscosity profile. *J. Phys. Oceanogr.,* **25**, 19–28. Find this article online

Lentz S. J., 2001: The influence of stratification on the wind-driven cross-shelf circulation over the North Carolina Shelf. *J. Phys. Oceanogr.,* **31**, 2749–2760. Find this article online

MacCready P., and P. B. Rhines, 1993: Slippery bottom boundary layers on a slope. *J. Phys. Oceanogr.,* **23**, 5–22. Find this article online

Mellor G. L., and T. Yamada, 1982: Development of a turbulence closure model for geophysical fluid problems. *Rev. Geophys. Space Phys.,* **20**, 851–875. Find this article online

Price J. F., R. A. Weller, and R. Pinkel, 1986: Diurnal cycling: Observations and models of the upper ocean response to diurnal heating, cooling, and wind mixing. *J. Geophys. Res.,* **91**, 8411–8427. Find this article online

Send U., R. C. Beardsley, and C. D. Winant, 1987: Relaxation from upwelling in the Coastal Ocean Dynamics Experiment. *J. Phys. Oceanogr.,* **17**, 1683–1698. Find this article online

Smith R. L., 1995: The physical processes of coastal ocean upwelling systems. *Upwelling in the Ocean: Modern Processes and Ancient Records,* C. P. Summerhayes, K.-C. Emeis, M. V. Angel, R. L. Smith, and B. Zeitzschel, Eds., John Wiley and Sons, 39–64.

Trowbridge J. H., 1992: A simple description of the deepening and structure of a stably stratified flow driven by a surface stress. *J. Geophys. Res.,* **97**, 15529–15543. Find this article online

---

APPENDIX

6. The Role of Mixing

The assumption that the surface mixed layer depth is approximately $Z_0 + \Delta Z/2$ breaks down when there is significant deepening of the mixed layer. This can be quantified by comparing the amount of deepening during a model run to the initial thickness of the surface mixed layer. The amount of deepening can be estimated and scaled empirically from the model data. No previous work on mixed layer development addresses the specific configuration used in this modeling study, but a few

papers address similar scenarios. Perhaps the closest is that of Trowbridge (1992), who solved for the deepening of a surface mixed layer due to the input of surface stress in the absence of rotation. The scaling that Trowbridge proposes for the deepening rate:

$$h_t = \frac{3}{2}\frac{\mathrm{Ri}_c^{1/2}u_*^2}{B^{1/2}}, \tag{A1}$$

where $B = \rho^{-1} g \int \delta\rho \, dz$ is the integrated buoyancy anomaly of the upper layer, $\mathrm{Ri}_c = 1/4$ is a critical Richardson number, and $u_* = (\rho_0^{-1}\tau^s)^{1/2}$ is the surface friction velocity, agrees qualitatively with the modeled deepening rate. However, by comparing this scaling to that modeled in a set of runs with a wide range of initial parameters, the quantitative rate of deepening in the model tends to be about 5% of that predicted by this scaling. This may be due to the absence of rotation in the Trowbridge scaling, or the fact that the initial condition is different, with Trowbridge (1992) assuming a two-layered fluid, while the model has a strong pycnocline. The deepening rate in the model runs can then be estimated as

$$h_t = \beta\frac{3}{2}\frac{\mathrm{Ri}_c^{1/2}u_*^2}{B^{1/2}}, \tag{A2}$$

where $\beta = 0.05$ is a proportionality constant. The buoyancy B is constant in time since the density difference lessens as the depth of the mixed layer deepens. This implies that the deepening rate should be approximately constant in time, and that the amount of deepening is therefore proportional to the duration of the wind event. This scaling is not appropriate when surface heat flux plays a major role in determining the mixed layer depth (Price et al. 1986), but it does allow inconsistencies between the analytical scalings and the model runs to be rationalized in this particular scenario.

The appropriate scaling, to determine whether a given model run is going to experience significant deepening, is

$$\frac{h_t \Delta t}{Z_S}, \tag{A3}$$

where Δt is the duration of the run. If this fraction is large, the deepening is significant compared to the initial mixed layer depth. Conversely, if it is small, the deepening does not significantly affect the model response. For the base case, for a model run of five days, this value is 0.4, suggesting that the mixed layer deepens around 4 m over the course of the model run, and that the velocity estimate should be an overestimate by approximately 20%. For runs with stronger forcing or less stratification, the deepening should be proportionally greater.

Figures
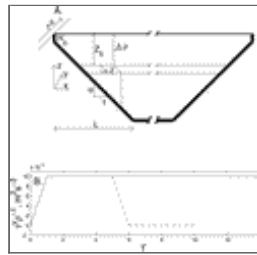
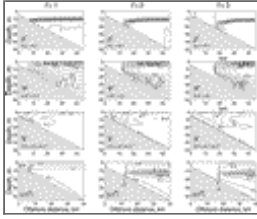Click on thumbnail for full-sized image.

FIG. 1. The basic physical configuration of the model. (a) The channel geometry, along with the definitions of the parameters determining the bathymetry (α, the bottom slope; L, the width of the sloped region; and H_0, the coastal wall depth), and the initial stratification (Z_0, the initial surface mixed layer depth; $\Delta\rho$, the density difference across the pycnocline; and ΔZ, the initial thickness of the pycnocline). The stratification is initially horizontally uniform. (b) The wind forcing used in the model. Solid line, continuous forcing; dashed line, transient forcing. Time units are inertial periods
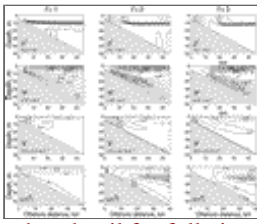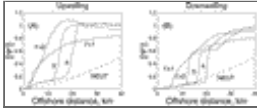
Click on thumbnail for full-sized image.

FIG. 2. Instantaneous fields of density, streamfunction, alongshore velocity, and internal stress at 1, 2, and 3 inertial periods during upwelling. The displays of density, streamfunction, and bottom stress are scaled as discussed in the text. The region in which the internal stress is <1% of the surface stress is shaded
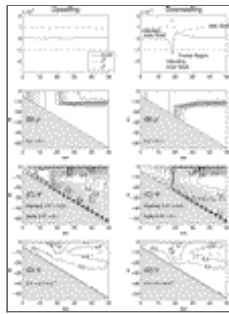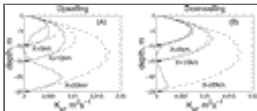

Click on thumbnail for full-sized image.

FIG. 3. Instantaneous fields of density, streamfunction, alongshore velocity, and internal stress at 1, 2, and 3 inertial periods during downwelling. The displays of density, streamfunction, and bottom stress are scaled as discussed in the text. The region in which the internal stress is <1% of the surface stress is shaded

Click on thumbnail for full-sized image.

FIG. 4. The maximum value of the streamfunction Ψ as a function of cross-shelf distance, plotted at 1, 2, 3, and 4 inertial periods. Dashed line is $\|\Psi\|$ for the neutral (unstratified) case. (a) Upwelling. (b) Downwelling

Click on thumbnail for full-sized image.

FIG. 5. (a: top panels) The terms of the vertically integrated alongshore momentum balance at $t' = 3$ for upwelling (first column) and downwelling (second column). The next three fields duplicate those in Fig. 2 ⊙, for reference. (b) The density field. (c) The alongshore velocity. (d) The cross-shelf streamfunction

Click on thumbnail for full-sized image.

FIG. 6. Profile of the vertical eddy viscosity, K_M, at 5 km, 10 km, and 20 km offshore after three inertial periods. Dashed line is profile in the neutral case, for comparison. (a) Upwelling. (b) Downwelling
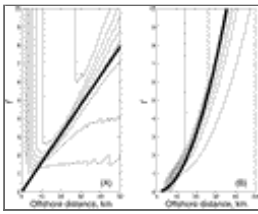
FIG. 7. Comparison of offshore propagation of the upwelling and downwelling fronts for the base case. (a) The surface density field during upwelling as a function of cross-shelf position and time; (b) the bottom density field during downwelling as a function of cross-shelf position and time. The heavy solid lines are the scalings (18; upwelling) and (26; downwelling)
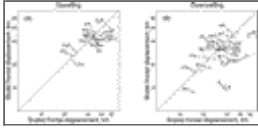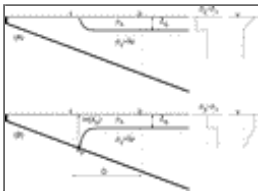
FIG. 8. (a). The displacement of the upwelling front between $t' = 2$ and $t' = 8$ for the upwelling case vs the displacement scale of Eq. (18). (b) The displacement of the downwelling front at $t' = 8$ vs the Ekman model [Eq. (25), symbol x] and barotropic model [Eq. (23), symbol o]
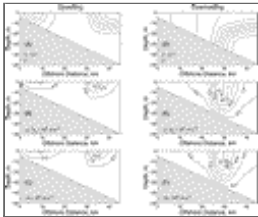
FIG. 9. Contoured fields of (a) the density field, (b) the pressure gradient term $(\rho^{-1}_0 p_x)$, and (c) the Coriolis term $(-f\upsilon)$, at 10 inertial periods (after a five inertial period wind event) in the transient case. (d)–(f) Same as (a)–(c) for downwelling case

FIG. 10. Calculating the alongshore geostrophic transport in the (a) upwelling and (b) downwelling case. Included for each is a simple schematic and the vertical distributions of density difference and alongshore velocity between the two points (1) and (2)
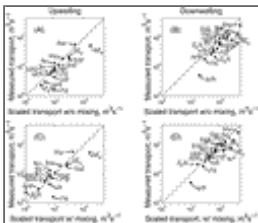
FIG. 11. The measured alongshore geostrophic transport in the upwelling and downwelling jets compared with the transport scalings with and without mixing. (a) Upwelling, no mixing. (b) Downwelling, no mixing. (c) Upwelling with mixing. (d) Downwelling with mixing
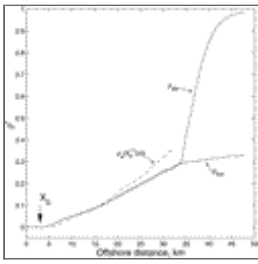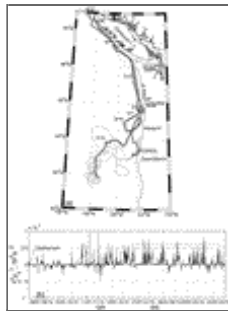
Click on thumbnail for full-sized image.

FIG. 12. Cross-shelf density structure in the model and from scaling on the inner shelf at $t' = 3$. The water on the inner shelf (onshore of the front, in this case approximately 31 km offshore) is vertically homogeneous. The solid lines are the surface and bottom density distributions, as indicated. The initial position of the pycnocline is specified by X_0.
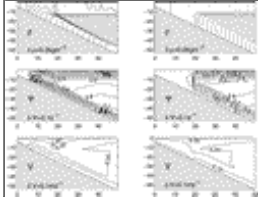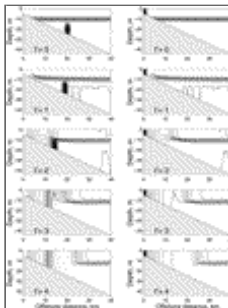

Click on thumbnail for full-sized image.

FIG. 13. The density, cross-shelf streamfunction, and alongshelf velocity at $t' = 3$ in a run with continuous stratification ($N = 0.02$ s^{-1}). First column: upwelling. Second column: downwelling.
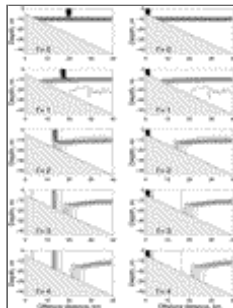

Click on thumbnail for full-sized image.

FIG. 14. (a) The paths of two drifters released on 24 Aug 1994, within 4 km of each other. The 200-m isobath is shown in gray. The position of the CARO3 NDBC meteorological station is marked with a star. The filled dots represent the deployment positions. The open circles are representative positions with dates of drifter 22252. The thickened lines correspond to the time periods shown in (b), and represent the portion of the time series when the floats are moving rapidly onshore or poleward. (b) The alongshelf wind stress at station CARO3. Positive is downwelling favorable. The solid lines correspond to time periods of rapid onshore or poleward movement of the drifters, marked as thick lines in (a).
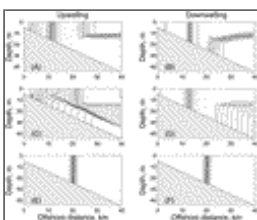

Click on thumbnail for full-sized image.

FIG. 15. Evolution of a passive tracer patch during base case upwelling at $t' = 0, 1, 2, 3, 4$. Shading represents tracer concentration, contours are isopycnals. Column 1: Tracer patch initially below pycnocline and offshore of upwelling front. Column 2: Tracer patch initially uniform over nearest 2 km to shore.

Click on thumbnail for full-sized image.

FIG. 16. Evolution of a passive tracer patch during base-case downwelling at $t' = 0, 1, 2, 3, 4$. Shading represents tracer concentration, contours are isopycnals. Column 1: tracer patch initially above pycnocline and offshore of downwelling front. Column 2: Tracer patch initially uniform over nearest 2 km to shore.

Click on thumbnail for full-sized image.

FIG. 17. The distribution of a patch of passive tracer at $t' = 4$ in the following cases: (a) strong pycnocline case, upwelling; (b) Strong pycnocline case, downwelling; (c) continuous stratification case, upwelling; (d) continuous stratification case, downwelling; (e) neutral (unstratified) case, upwelling; (f) neutral case, downwelling. Strong pycnocline cases are redundant with $t' = 4$ in Figs. 15 ⊙▬ and 16 ⊙▬, but are included for easy comparison.

Corresponding author address: Jay A. Austin, Center for Coastal Physical Oceanography, Crittendon Hall, Old Dominion University, Norfolk, VA 23529-0276. E-mail: jay@ccpo.odu.edu

top ▲